Hyperfine structure, isotopic level shifts, and pressure self-broadening of the $7\,^2P$ states of natural thallium by Doppler-free two-photon absorption*

A. Flusberg, T. Mossberg, and S. R. Hartmann
Columbia Radiation Laboratory, Department of Physics, Columbia University, New York, New York 10027
(Received 9 July 1976)

The hyperfine constants, isotopic level shifts, and a pressure self-broadening constant of the $7\,^2P$ states of ^{203,205}Tl have been measured by the Doppler-free two-photon absorption technique. The hyperfine constant of the $7\,^2P_{3/2}$ state is found to be greater than that of the $6\,^2P_{3/2}$ state. This anomaly is tentatively attributed to a sign change in the promoted core s-electron spin-polarization contribution to the hfs as calculated by Fermi and Segrè for the $6\,^2P_{3/2}$ state. The isotope shift of the $7\,^2P_{1/2}$ state is 20% smaller than that of the $7\,^2P_{3/2}$ state, confirming the nuclear volume effect of the $p_{1/2}$ electron. At higher pressures line broadening is observed as the Tl density is increased.

I. INTRODUCTION

The atomic structure of neutral thallium is simple inasmuch as it is characterized by a single p electron outside of otherwise closed shells and subshells. The two isotopes which occur in nature, ^{203}Tl (29.5%) and ^{205}Tl (70.5%), both have a spin-$\frac{1}{2}$ nucleus. Thus the hyperfine-interaction Hamiltonian consists only of the single magnetic dipole term $A_J \vec{I}\cdot\vec{J}$, where $\vec{I}$ is the nuclear spin and $\vec{J}$ is the total electronic angular momentum. In the absence of an external magnetic field the $^2P_{1/2}$ and $^2P_{3/2}$ multiplets split into two levels, the $^2P_{1/2}$ into a $F=0$ and a $F=1$ level, and the $^2P_{3/2}$ into a $F=1$ and a $F=2$ level (see Fig. 1). Although the large charge of the Tl nucleus introduces relativistic effects, these are readily taken into account by the semiempirical relativistic single-valence-electron theory of Casimir,[1,2] which appears able to account for the hyperfine structure (hfs) of all the hitherto measured $n\,^2P_{1/2,\,3/2}$ ($n=6, 8, 9, 10$) states except the $6\,^2P_{3/2}$ state. For this state the single-valence-electron theory overestimates the size of the hfs by an order of magnitude. This was explained by the pioneering work of Fermi and Segrè,[3] who showed that the mixing of the $6s7s6p$ configuration with the $6s^26p\,^2P_{3/2}$ state could provide the requisite spin density at the nucleus to nearly cancel the contribution of the single $p_{3/2}$ electron.

For the $n=6$ ground ^2P states Schwartz[4] has improved upon the Casimir work by using the more realistic (but still semiempirical) screened potential of Tietz and has found that the hfs interaction constants of the $6\,^2P_{1/2}$ ($6\,^2P_{3/2}$) state should be increased (decreased) by about 20% over the Casimir values. This result was important in two respects: First, the spin-polarization contribution (of the type calculated by Fermi and Segrè) now required for agreement with experiment was reduced by 30%; and second, the Schwartz result led to a calculated $6\,^2P$ hfs isotope anomaly in agreement with experiment.[5] For $n=8, 9, 10$ Odintsov[6] measured $n\,^2P$ hyperfine constants which were in rather good agreement with the Casimir theory; in the light of the Fermi-Segrè result this was somewhat surprising. Unfortunately, the atomic-beam method (used by Odintsov) did not allow a study of the $7\,^2P$ states, since it would have required a sensitive infrared detector to monitor the spectrum of the decay to the lower $7\,^2S_{1/2}$ state. The advent of the Doppler-free two-photon absorption (TPA) technique[7] eliminates this necessity. Using this technique, we find that for the $n=7$ states the hyperfine constants have those values which would be inferred from a simple extrapolation of Odintsov's results plotted against the fine-structure splitting, which is the natural variable of the Casimir theory. What is unusual about this result is that it yields a hyperfine constant for the $7\,^2P_{3/2}$ state which is greater than that of the $6\,^2P_{3/2}$ state.[8]

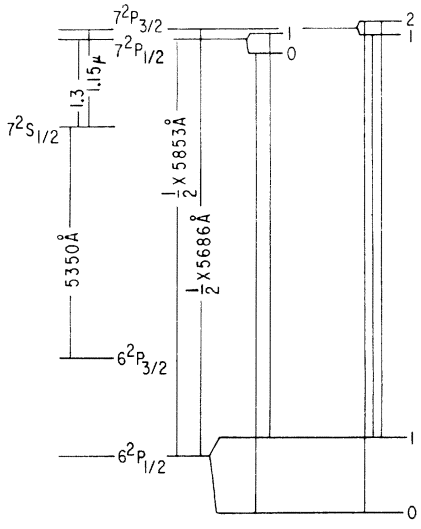

FIG. 1. Energy levels relevant to the $6\,^2P_{1/2}$-$7\,^2P_{1/2,3/2}$ two-photon absorption experiment.

There are several other states of thallium[8(a)] and indium[8(b)] for which the hyperfine constant increases in magnitude when the principle quantum number is increased by 1 unit, but in all these cases, strong mixing with a nearby configuration is believed to be responsible for the anomaly. In contrast, there appear to be no perturbing configurations energetically "close" to either $7\,^2P$ or $6\,^2P$ terms of thallium.

We analyze the existing hfs data for the ^2P states in Tl using Schwartz's theory for $n=6$ and Casimir's theory for $n>6$. Following Schwartz, we assume that departures from calculated hfs constants arise from promotion of core s and p electrons, and we use the experimental hfs data and the theoretical semiempirical values of the hfs constants to determine the fractional contribution to the hfs constants from both these processes. We find that the relative contribution of these processes is roughly independent of principal quantum number and that the anomalous behavior of the $6\,^2P_{3/2}$ state is due to a sign change in the spin-polarization contribution from the promoted core s electron.

Our measurements also show that the isotope shift of the $7\,^2P_{1/2}$ state is significantly smaller than that of the $7\,^2P_{3/2}$ state. This behavior, which is similar to that found in the $6\,^2P$ states,[2,9,10] supports the idea that the isotope shifts of the $^2P_{1/2}$ states receive a significant contribution from the $p_{1/2}$ electrons.

We detect the two-photon absorption by monitoring fluorescence to the nearly unpopulated $6\,^2P_{3/2}$ state. The reduced self-absorption allows us to work at considerably higher vapor pressures than would otherwise be possible (or than would be possible by the atomic-beam method). We have found that the two-photon linewidth increases linearly with pressure when the Tl pressure is increased above that corresponding to 10^{15} atoms cm^{-3}. This result is interpreted in terms of nonresonant thallium-thallium collisional broadening.

Before discussing the above results in detail, we will describe the experimental apparatus and technique. We also include a section on our observation of the splitting of the two-photon absorption lines in a weak magnetic field. Finally we have included two appendices in which we (i) calculate the relative two-photon absorption rates between different Zeeman and hyperfine levels, and (ii) estimate the overall two photon absorption rate.

II. APPARATUS

The experimental apparatus required in the Doppler-free two-photon absorption (TPA) technique is relatively modest and easily accessible to most research laboratories. It consists of a laser, a container for the material to be studied, and a suitable detector which records the absorption taking place. This simplicity has attracted considerable interest, and since its experimental verification in 1974,[11-13] the technique has been used to measure hyperfine splittings, isotope shifts, dc[14] and optical[15] Stark shifts, and magnetic field splittings[16] in several atomic vapors. Many of the experiments reported to date have either employed high-peak-power pulsed lasers or have taken advantage of a nearly resonant intermediate state to enhance the TPA cross section. We work at higher atomic densities to compensate for our nonresonant interaction (~8000-cm^{-1} mismatch) and weak laser excitation (~100 mW).

The thallium vapor was contained in an oven-heated fused-silica cylindrical cell 15 cm in length and 2.5 cm in diameter. The cell was prepared by a bakeout at 1050 °C for 30 hours, after which thallium of 99.9999% metallic purity was doubly distilled into it. Care was taken during the introduction of the thallium to avoid contamination by thallium oxide. The oven was placed in a solenoid so that a dc magnetic field could be applied along the cell axis.

A schematic diagram of our apparatus is shown in Fig. 2. The cw single-mode dye laser (Spectra Physics 580) is pumped by 2 to 3 W of 5145-Å radiation from a cw argon-ion laser and is adjusted to lase at either 5853 or 5686 Å. The "580" laser can be electronically scanned in frequency. The 5853- and 5686-Å radiation is linearly polarized and its frequency is about 8000 cm^{-1} from the $6\,^2P_{1/2}$-$7\,^2S_{1/2}$ transition frequency (see Fig. 1). The laser beam is focused into and traverses the sample cell. It is then reflected back on itself by a corner-cube and focused down again so that good spatial overlap occurs between the oppositely propagating beams in a volume about 0.01 cm in diameter and 2 cm in length.

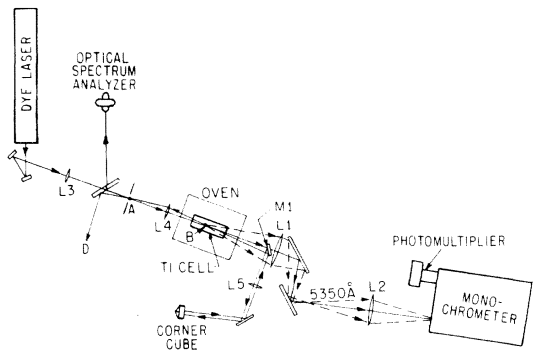

FIG. 2. Schematic of the TPA experiment (see text).

With the combination of the corner-cube and lenses L_3, L_4, and L_5, the opposing beams can be made to cross at an angle of about 10 mrad; the reflected beam is then spatially separate from the incident beam at the laser, and feedback from the reflected beam into the laser is avoided. In addition, this scheme provides good, relatively alignment-free spatial overlap, which may be monitored during setup by placing a 100-μm diam pinhole at A, a point conjugate to the overlap point B, and observing the relative intensity of the reflected beam passing through the pinhole.

The beam-overlap volume is imaged by lenses L_1 and L_2 onto the entrance slit of a grating monochrometer. Mirror M_1, which is 1 cm in diameter, serves as a laser-beam stop aside from its function as reflector. Our signal, consisting of $7^2S_{1/2}$-$6^2P_{3/2}$ 535.0-nm fluorescence emitted around mirror M_1 in the forward direction, is isolated by the monochrometer and detected by an EMI 9635QB photomultiplier tube. The advantage of monitoring the TPA at 535.0 nm is that the sample cell is optically thin at this wavelength, since the $6^2P_{3/2}$ terminal level is 7793 cm^{-1} above the ground $6^2P_{1/2}$ level and is therefore only slightly populated. This allows us to work at much higher number densities than would otherwise be possible.

The output of the photomultiplier as a function of incident dye-laser wavelength is displayed on an oscilloscope. Signal, consisting of several narrow lines on a Doppler-broadened background (see Fig. 3), is observed at a dye-laser power of approximately 100 mW (inside the thallium cell) and a thallium vapor pressure of about 80 mTorr or greater. The narrow-line signal has the expected characteristics of Doppler-free TPA, disappearing when the retroreflected laser beam is blocked and varying as the square of the incident laser intensity. The signal is large enough so that there is no need of synchronous detection, and in fact so large that it can be detected while sweeping the dye-laser frequency through a single Doppler-free absorption line in a few hundred microseconds, a time short compared to the period of most of the dye-laser noise. Thus it is possible to observe an atomic absorption linewidth of less than 12 MHz [full width at half-maximum (FWHM)] on a single sweep.

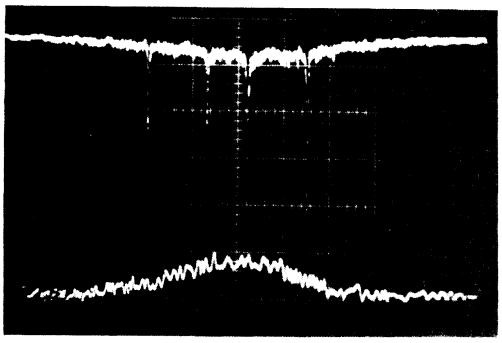

FIG. 3. *Upper trace*: 535-nm fluorescence as a function of dye-laser frequency (increasing to the right), showing the $6^2P_{1/2}$-$7^2P_{3/2}$ TPA spectrum ($F=1\rightarrow 1$ and $1\rightarrow 2$ only). Horizontal scale: 240 MHz/div. The smaller (larger) peaks correspond to ^{203}Tl (^{205}Tl). (Cf. Fig. 5). Note the Doppler-broadened backround. *Lower trace*: Transmission of the dye laser through an iodine vapor cell; again note the Doppler-broadened absorption. Both traces were obtained on a single sweep (at about 20 msec/div) of the dye-laser frequency, as observed on a dual-beam oscilloscope.

Identification of the lines was made from the known ratio of abundances of the two thallium isotopes and from the theoretical ratio of absorption rates of the various hyperfine transitions. As we show in Appendix A, these theoretical ratios depend only on angular momentum coupling factors relating the initial ($6^2P_{1/2}$) and final ($7^2P_{1/2,3/2}$) states. The $F=1\rightarrow 1$ and $F=1\rightarrow 2$ $6^2P_{1/2}\rightarrow 7^2P_{3/2}$ transitions, which have equal absorption rates, were identified with certainty from their splittings in a weak axial magnetic field.

The dye-laser frequency could also be electronically tuned by hand either continuously over a span of about 1 GHz or in discrete 508-MHz jumps over a range of several tens of GHz. The frequency jumps occurred when the spacing of an intracavity etalon was adjusted piezoelectrically to choose successive laser-cavity modes. The mean frequency difference $\Delta\nu_M$ between successive modes (mode jumps) was found to be constant to within 1 MHz (see Sec. III) as long as the cavity length was not significantly altered, as one expects from the formula $\Delta\nu_M = c/2L$, where c is the velocity of light and L the optical length of the laser cavity.

III. EXPERIMENTAL METHOD: FREQUENCY-DIFFERENCE MEASUREMENTS

Part of the dye-laser beam was split off by a beam splitter and was incident on an optical spectrum analyzer (Spectra Physics model 470) having a nominal spectral range of 8 GHz. A triangular ramp voltage applied continuously at about 25 Hz to the piezoelectric holder of one of the spectrum-analyzer mirrors swept the interferometer resonance frequency through somewhat less than three spectral ranges. Since the dye laser oscillated in a single axial mode, the transmission of the interferometer, observed on an oscilloscope sweeping synchronously with the

ramp voltage, consisted of narrow peaks separated (apparently) by the spectrum-analyzer spectral range $\Delta\nu_{SA}$. The horizontal sweep of this oscilloscope could thus be calibrated in terms of $\Delta\nu_{SA}$.

Differences in frequency between any two two-photon resonances were measured as follows: The dye-laser frequency was electronically tuned to the center of the first absorption, while the transmission of the (swept) spectrum analyzer was continuously displayed on an oscilloscope. The laser frequency was then tuned by an integral number of mode jumps $\Delta\nu_M$ until its frequency was as close as possible (within 300 MHz) to the second absorption line. After the position on the oscilloscope sweep at which the laser frequency was resonant with the spectrum analyzer (the position of peak transmission) had been noted, the laser frequency was tuned continuously to the second two-photon absorption line, and the new position of peak transmission was noted. The difference $\Delta\nu$ between the two absorption frequencies was thus measured in terms of $\Delta\nu_M$ and a measured small fraction of the spectrum-analyzer spectral range. The measurement was repeated many times, successive measurements being made from the first absorption to the second and back to the first. By this means the measurement of $\Delta\nu$ was corrected for spectrum-analyzer as well as laser frequency drift. (Both were on the order of several tens of MHz per minute).

The laser mode jump $\Delta\nu_M$ was measured in terms of $\Delta\nu_{SA}$ as follows: The position of a transmission peak on the oscilloscope sweep was noted before and after the laser frequency was tuned discretely by $16\Delta\nu_M$. The number 16 was chosen because of the near-coincidence between $16\Delta\nu_M$ and the spectrum-analyzer spectral range. By using an expanded oscilloscope scale, we were able to measure the difference between $16\Delta\nu_M$ and $\Delta\nu_{SA}$ reproducibly to within 10–20 MHz.

Finally, the spectral range $\Delta\nu_{SA}$ was measured by comparison with the 7.866-GHz spectral range of a plane-parallel Fabry-Perot interferometer, the fixed spacing of which was accurately known. To make the comparison, we used the method described above for the measurement of the frequency difference between two absorptions, utilizing the dye laser as a light source incident simultaneously on both interferometers.

Some discussion of the sources of error in this method of measurement of frequency differences is in order. Location of the central frequency of each two-photon absorption was limited by the inherent linewidth of the absorption as well as by laser frequency jitter. The former arises from the natural and collisional atomic lifetime of the excited 7^2P level and from the rms time of flight

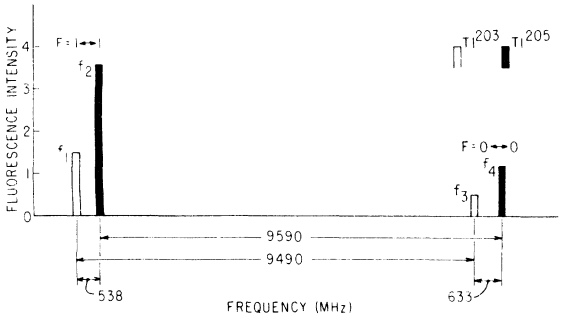

FIG. 4. TPA spectrum, $6^2P_{1/2}-7^2P_{1/2}$. The indicated frequency splittings are approximate and are based on our measurements (see Table I).

in the 100-μm-diam, 2-cm-long overlap volume. At a thallium vapor pressure of approximately 100 mTorr, at which the frequency-difference measurements were made, the main contribution to the linewidth came from the laser jitter of about ± 12 MHz. This jitter, which appeared as fluctuations in the position of the transmission peak, also limited the measurement of the peak position. Finally, the assumption of linearity of the spectrum-analyzer sweep was used to make the frequency-difference measurements. However, the method employed necessitated measurement of frequency differences which were always smaller than about 300 MHz, which constituted less than 4% of a spectral range, and only about 1% of the full spectrum-analyzer sweep. We estimate the possible percentage error due to nonlinearity over this small a sweep range as about 3%, i.e., 9 MHz in 300. Since we averaged our data over several positions in the spectrum-analyzer sweep, we do not believe that the sweep nonlinearity contributed any appreciable systematic error to the average of the data.

The measured values of the various frequency intervals are depicted in Figs. 4 and 5 and are listed in Table I. From them we have calculated

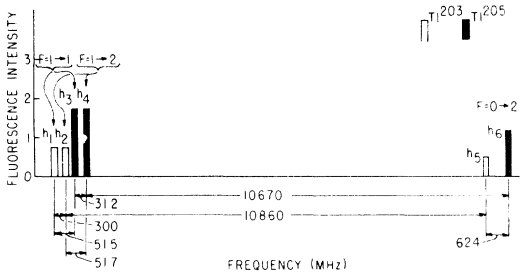

FIG. 5. TPA spectrum, $6^2P_{1/2}-7^2P_{3/2}$. The indicated frequency splittings are approximate and are based on our measurements (see Table I).

TABLE I. Measured frequency difference between various two-photon transitions.

Transition	Frequency interval	Measured value (MHz)
$6\,^2P_{1/2}$-$7\,^2P_{1/2}$	$f_2-f_1\equiv f_{21}$ [a]	537.9(4.1) [b]
	f_{43}	633(9)
	f_{42}	9590(30)
$6\,^2P_{1/2}$-$7\,^2P_{3/2}$	h_{31}	515.3(2.8)
	h_{42}	517.3(3.1)
	h_{32}	215(18)
	h_{43}	312(9)
	h_{64}	10 669(19)
	h_{65}	624(12)

[a] See Figs. 4 and 5 for definition.
[b] Numbers in parentheses denote standard deviations.

the hyperfine splittings and isotope shifts of the $7\,^2P_{1/2}$ and $7\,^2P_{3/2}$ states. They are given in the upper half of Fig. 6. As an independent check on our measurements, we may compare our observed value of the $6\,^2P_{1/2}$ hyperfine constants with the high-precision microwave measurements of Lurio.[17] From our measurement of the $6\,^2P_{1/2}$-$7\,^2P_{3/2}$ spectrum we obtain $A_{205}=21\,339(38)$, $A_{203}=21\,126(45)$, and $A_{205}-A_{203}=213(25)$. Our values are consistent with those of Lurio to within our experimental error (see Fig. 6).

IV. ANALYSIS OF hfs DATA

The relativistic semiempirical theory of Casimir[1,2] relates the hfs constant $a_j(n)$ of a single-valence p_j-electron atom with principal quantum number n to the derivative dW/dn of term energy with respect to n, as follows:

$$a_j(n)=\frac{\alpha^2}{3}g_I'Z_i\frac{F_r(j,Z_i)}{j(j+1)}\left(\frac{-dW_n}{dn}\right). \tag{1}$$

Here α is the fine-structure constant, g_I' the reduced nuclear g factor, Z_i the shielded nuclear charge, and F_r a relativistic correction factor. To correct for the penetration of the $p_{1/2}$ electron into the nucleus, $a_{1/2}$ should be multiplied by an additional factor $(1-\delta)(1-\epsilon)$.[2] dW_n/dn is obtained from a plot of the term energies of the ^2P series against n, while Z_i is obtained from a plot of the fine-structure splittings $\delta\nu_n$ against dW_n/dn. According to the Casimir theory the Landé formula[18] $\delta\nu_n=(\alpha Z_i)^2W_n^{3/2}/2$ should be replaced by

$$\delta\nu_n=\frac{(\alpha Z_i)^2}{4}\mathcal{K}_r(Z_i)\left(\frac{-dW_n}{dn}\right), \tag{2}$$

where $\mathcal{K}_r$ is a relativistic factor. Equations (1) and (2) imply a linear relationship between $a_j(n)$ and $\delta\nu_n$, which for thallium with $Z_i=76.5$ (see below), $g_I'=1.755\times10^{-3}$ (^{205}Tl),[19] and $(1-\delta)(1-\epsilon)=0.95$,[2] yields $a_{1/2}(n)=(6.9\times10^{-5})\delta\nu_n$, $a_{3/2}=(8.0\times10^{-6})\delta\nu_n$.

We have listed the known hfs data for the ^2P states of Tl in Table II, and in Fig. 7 we show a log-log plot of the hyperfine constants for the $J=\frac{1}{2}$ and $\frac{3}{2}$ states, respectively, as a function of fine-structure splitting. In agreement with the Casimir theory, the data (except for $n=6$) fit closely to a straight line of unit slope. Indeed, the Casimir theory also succeeds in predicting the magnitude, the straight lines in Fig. 7 being Casimir's results for a shielded nuclear charge $Z_i=76.5$. For $J=\frac{1}{2}$ experiment and theory agree to within a few percent (for $n>6$) while for $J=\frac{3}{2}$ the experimental values are of the order of 50% too high. For $n=6$ the disagreement between theory and experiment is marked, in particular for $J=\frac{3}{2}$, for which experiment yields a hyperfine interaction constant $A_{3/2}$ which is an order of magnitude too small. This discrepancy is understood from the work of Fermi and Segrè to be due to the contribution to the hfs from the $6s7s6p$ state, which is mixed in with the ground $6s^26p$ configuration by the exchange part of the interelectron Coulomb interaction (spin polarization).[3] Fermi and Segrè were able to show that the spin-polarization contribution to $A_{3/2}$ for the $6\,^2P_{3/2}$ state was of the same order as and of opposite sign to the contribution of the valence electron. The corresponding effect on the $J=\frac{1}{2}$ state is fractionally smaller because the single-valence-electron value of $A_{1/2}$ is an order of magnitude larger than that of $A_{3/2}$.

Aside from the effects of configuration interactions the relativistic single-electron theory does

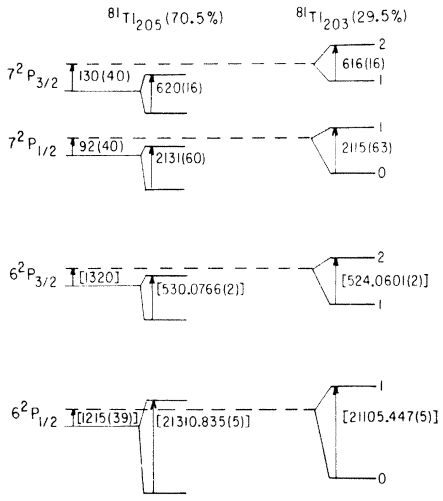

FIG. 6. Hyperfine splittings and isotope shifts (in MHz) of the $6\,^2P$ and $7\,^2P$ states of thallium, with reported error bars. Numbers in brackets were obtained from other works (see Table II), while all other numbers are based on this work.

TABLE II. Tl $n\,^2P_J$ isotope shifts and ^{205}Tl hyperfine splittings (in 10^{-3} cm^{-1}).

Principal quantum number n	Experimental isotope shift $J=\frac{3}{2}$	$J=\frac{1}{2}$	Experimental splittings $2A_{3/2}$	$A_{1/2}$
6	−44.0 [b]	−40.5(1.3) [c]	17.68 [d]	710.8 [e]
7 [a]	−4.3(1.3)	−3.1(1.3)	20.68(0.53)	71.1(2.0)
8 [b]	−0.8	−0.4	8.7	26.3
9 [b]	−0.1	+1.1	3.5	13.1
10 [b]	0	...	2.3	...

[a] This work.
[b] Reference 6.
[c] Reference 9.
[d] Reference 5.
[e] Reference 17.

very well in connecting theory with experiment, and many measured ^2P-state properties in Tl seem to be simply described. For example, if we express the term energy W (in rydbergs) by the Rydberg-Ritz formula[20]

$$W = 1/(n^*)^2 , \tag{3}$$

where

$$n^* = n - a - bW_n - cW_n^2 \tag{4}$$

and W_n are the experimental values,[21] then for $a = 4.182$, $b = 0.4313$, and $c = 0.4516$ the fractional differences between W and W_n are less than 0.2% for all n such that $6 \leq n \leq 11$. Since relativistic effects are important, the Landé formula for the fine-structure splitting $\delta\nu$ should, according to Casimir, be replaced by Eq. (2). The improvement gained by the Casimir theory is shown in Fig. 8, where we have compared plotting experimental values of[21] $\delta\nu$ as a function of $W^{3/2}$ (Landé's theory) with the corresponding plot as a function of dW/dn (Casimir's theory) using Eqs. (3) and (4). For $7 \leq n \leq 11$ the Casimir theory works very well; normalization is obtained using $Z_i = 76.5$. We take this good behavior as support for the use of Casimir's formula for the hfs for the ^2P states in Tl for $n = 7, 8, 9, 10$. For $n = 6$, $\delta\nu$ deviates from the straight-line fit and Casimir's formula would be more suspect. Fortunately, Schwartz has significantly improved upon the Casimir calculation for $n = 6$ by using the screened nuclear po-

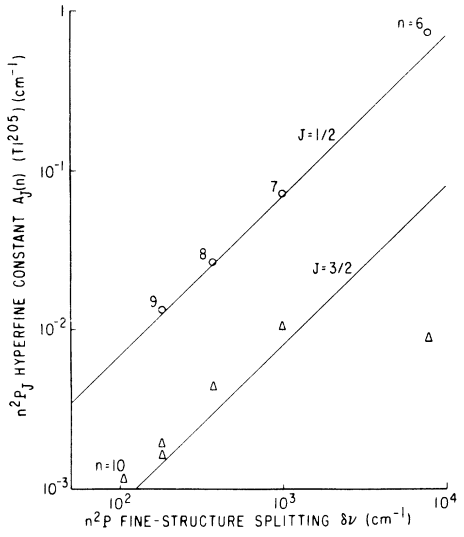

FIG. 7. Hyperfine constants vs fine structure of the $n\,^2P_{1/2}$ (circles) and $n\,^2P_{3/2}$ (triangles) series of ^{205}Tl. The two points drawn for $9\,^2P_{3/2}$ correspond to Odintsov's measured values of the hyperfine constants of ^{205}Tl and ^{203}Tl, which should be equal to within 1% but are not because of experimental error. The straight lines correspond to the Casimir theory.

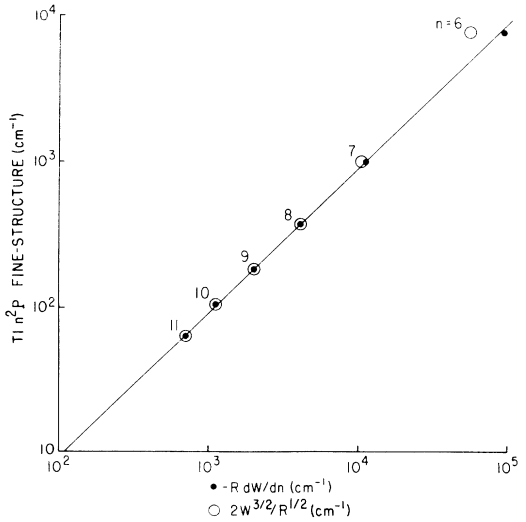

FIG. 8. Tl $n\,^2P$ fine-structure splitting as a function of dW/dn and $W^{3/2}$ (R is the Rydberg constant).

tential of Tietz to make a semiempirical calculation of the single-valence-electron wave functions.[4] He finds that the Casimir values need only be changed by ~20%. This relatively small correction can be taken as additional support for the Casimir work, and we are therefore motivated to use the differences between the experimental hfs values and the hfs values predicted by the semiempirical theory of Schwartz (for $n=6$) and Casimir (for $n=7, 8, 9$) in order to ascertain the spin-polarization contributions to the hfs. This is readily accomplished by writing the hfs constants in the form[4]

$$A_{1/2}=a_{1/2}(1-\gamma+R_p)+a_c \ , \tag{5}$$

$$A_{3/2}=a_{3/2}(1+R_p)-a_c \ , \tag{6}$$

where $a_{1/2,\,3/2}$ are the single-valence-electron hfs constants, R_p is the fractional contribution to $A_{1/2,\,3/2}$ from polarized core p electrons, and a_c is the contribution from the polarized core s electrons. The quantity $1-\gamma=(1-\delta)(1-\epsilon)$, ignored in Schwartz's work, corrects for the nuclear-charge and magnetic moment distribution of the finite-size nucleus; for Tl $\gamma\cong 0.05$.[2] In writing Eqs. (5) and (6) we have, following Schwartz, assumed that $p\rightarrow p'$ and $s\rightarrow s'$ excitations are the major contributors to the core polarization.[22] From Eqs. (5) and (6) we solve for R_p and a_c for each value of n, and we tabulate our results in Table III. The three major results are that R_p is of the order of $|a_c/a_{1/2}|$, $|a_c/a_{1/2}|$ and $|R_p|$ remain constant to within about a factor of 3, and the sign of a_c for $n=6$ is opposite to that for $n=7, 8, 9$. The sign change of a_c is not surprising in view of the fact that the various inner s shells may give nearly equal but opposing contributions to the total value of a_c.[22,23] In addition we should not expect $a_c/a_{1/2}$ to become very small with increasing n for the following reason: The fractional amount of promoted s-electron wave function is inversely proportional to an energy denominator $W'-W_n$, where W' is the energy of a higher-configuration state which is mixed into the n^2P state by the exchange terms of the interelectron Coulomb interaction.[3] This energy denominator decreases with increasing n. Thus the tabulated values of a_c and R_p seem reasonable and are large enough to motivate separate calculation. For $n=6$ the anomalous result arises from $a_c\simeq +a_{3/2}$.

We note that other authors[6,10] have proposed that the Tl $n\,^2P$ series ($n>6$) hyperfine constants are strongly perturbed by mixing of the various $6s^2n'p(n'\neq n)$ with each $6s^2np$ pure configuration, an effect associated with the nonvanishing of the off-diagonal matrix elements of the spin-orbit interaction. However, if this mixing were strong, one would not expect the experimental fine-structure constants to lie on the straight line (of slope 1) of Fig. 8, since the fine-structure constants are also expected to be perturbed by this type of configuration mixing (see Ref. 10). We have therefore ignored the possible contribution of this $np\rightarrow n'p$ mixing in our analysis.

In calculating R_p and a_c, we have also ignored the correction to the normalization of the $n\,^2P_{1/2}$ and $n\,^2P_{3/2}$ wave functions which arises from the difference between the n^2P term energy and the energy of each of these states. From the work of Casimir,[1] this leads to a fractional increase by approximately $3(\alpha Z)^2/(n-4)$ in the value of $a_{3/2}/a_{1/2}$ for the n^2P states of Tl. The deduced value of a_c (Table III) is then increased by (10—30)%, while that of R_p is decreased by (15—50)%. However, the basic conclusions of this section remain unchanged.

TABLE III. Summary of calculated hyperfine constants and deduced core-polarization corrections for ^{205}Tl (in 10^{-3} cm^{-1}).

Theory	n	Calculated $a_{1/2}$	Calculated $a_{3/2}$	Experimental $A_{1/2}$	Experimental $A_{3/2}$	R_P[a]	a_c
Schwartz	6	620	51	711	8.8	0.12	49
HF	6	626	46	711	8.8	0.12	43
OHFS	6	624	37	711	8.8	0.14	33
Casimir	6	562	62	711	8.8	0.20	65
Casimir	7	72	8.0	71.1	10.3	0.06	−1.9
Casimir	8	27	3.0	26.3	4.35	0.07	−1
Casimir	9	13	1.4	13.1	1.75	0.07	−0.2

[a]Dimensionless.

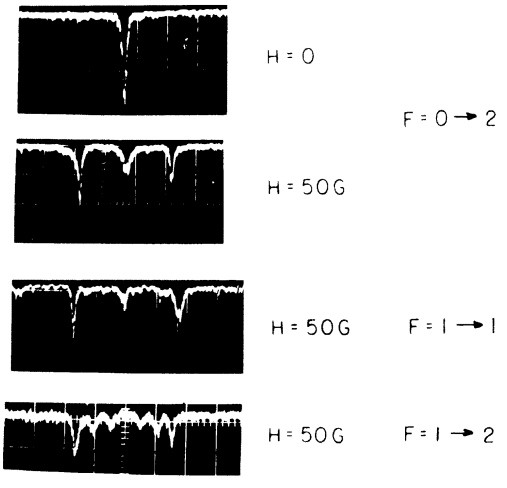

FIG. 9. ^{205}Tl $6\,^2P_{1/2}$-$7\,^2P_{3/2}$ TPA splitting in a weak axial magnetic field H for the three possible multiplet transitions. Each oscilloscope trace represents a single sweep of the laser frequency, increasing to the right at approximately 38 MHz/div. Time scale: 2 msec/div.

Fermi and Segrè[3] calculated an a_c of $+0.043$ cm^{-1} for $n=6$. This value, which was obtained using rough estimates of the physical parameters, was only to be thought of as an order-of-magnitude estimate. In particular, they considered mixing of only the $6s7s6p$ with the $6s^26p$ configuration in the $6\,^2P$ states. Nevertheless, their result agrees quite well with the value $a_c = 0.048$ cm^{-1} deduced from Schwartz's work. Lindgren and Rosen,[24] using Hartree-Fock wave functions, have also calculated the uncorrected hyperfine constants and their results are also listed in Table III. Their work supports that of Schwartz.

V. SPLITTING OF THE TPA SPECTRUM IN A WEAK MAGNETIC FIELD

Photographs of oscilloscope traces of $6\,^2P_{1/2}$-$7\,^2P_{3/2}$ TPA signal in the presence of a weak magnetic field applied along the direction of propagation of the laser are shown in Fig. 9. To obtain these traces, each of which represents a single oscilloscope sweep, the dye-laser frequency is swept at about 20 MHz/msec. and the oscilloscope sweep is triggered synchronously. On this time scale, laser FM noise contributes little artificial broadening to the linewidths. The FM noise does show up, however, as sweep-to-sweep jitter (of about ± 10 MHz) in the position of the TPA. It also contributes some nonlinearity to the frequency sweep.

The observed magnetic field splitting of the two-photon transitions was in agreement with the theoretical calculation of Appendix A. Thus, for the $6\,^2P_{1/2}$-$7\,^2P_{3/2}$ transition, the $F=0\rightarrow 2$, $F=1\rightarrow 1$, and $F=1\rightarrow 2$ lines were observed to split into 3, 3, and 6 components, respectively, the $M=\pm 1\rightarrow \pm 1$, $F=1\rightarrow 1$ transition being too weak for us to observe (see Table IV). The absence of the $M=0\rightarrow 0$ component from the $F=1\rightarrow 2$ transition, which is apparently not due to any selection rule, was also confirmed. The left-to-right asymmetry in the magnitude of the transitions, evident in Fig. 9, was found to reverse upon reversal of the magnetic field; it was probably due to a deviation of the retroreflected-beam polarization from linearity. Finally, no splitting or broadening of the $6\,^2P_{1/2}$-$7\,^2P_{1/2}$ transitions was observed in a magnetic field as high as 50 G, in agreement with theory (see Appendix A).

VI. ISOTOPE SHIFT

From our data we find an isotope shift in the TPA transition frequencies of 1123.2(7.7) and 1084.8(6.8) MHz, respectively, for the $6\,^2P_{1/2}$-$7\,^2P_{1/2}$ and $6\,^2P_{1/2}$-$7\,^2P_{3/2}$ transitions, respectively. In each case the heavier isotope has the higher transition frequency. To calculate the $7\,^2P_{1/2}$-state isotope shifts appearing in Table II we have used the ground-state isotope shift of Schuler,[9] whose value is in turn based on the measurements by Odintsov.[6] The latter defined all ^2P-state shifts with respect to the $10\,^2P_{3/2}$ state, making the reasonable assumption that the $10^2P_{3/2}$-state isotope shift is negligible compared to his experimental error (i.e., less than a few MHz). Like that of the $6\,^2P$-state isotope shifts, the sign of the $7\,^2P$ shifts is negative; that is, it is opposed to that expected from the theory of finite nuclear volume. It may be explained as occurring as a result of the shielding of the $6s^2$ electrons from the nucleus by the $7p$ electron.[2] Our measurements indicate that the $7\,^2P_{3/2}$ isotope shift is larger in magnitude than that of the $7\,^2P_{1/2}$ state by 38 ± 10 MHz. This may be explained as resulting from the nuclear-volume effect in the $7\,^2P_{1/2}$ state. As Fischer has discussed,[10] a similar situation exists for the $6\,^2P_{1/2,\,3/2}$ states.

VII. PRESSURE SELF-BROADENING

The linewidth of the $6\,^2P_{1/2}$-$7\,^2P_{1/2}$ $F=1\rightarrow 1$ transition (^{205}Tl) was observed as a function of the central temperature of the thallium cell in the temperature range 690–860 °C. To minimize artificial broadening associated with laser FM noise, we made the linewidth measurements by sweeping the laser frequency at about 50 MHz/msec, so that a 10-MHz-wide line was traversed in only 200 μsec. The temperature was measured by a Platinel thermocouple located near the outer surface of the cell. It was found that the linewidth increased reversibly as the temperature was increased.

The following sources (other than laser frequency jitter) may contribute to the observed absorption linewidth:

(a) The natural lifetime of the $7\,^2P_{1/2}$ state, associated with decay to the $7\,^2S_{1/2}$ state. A Coulomb-approximation calculation, utilizing the tables of Bates and Damgaard,[25] yields 6.1 MHz FWHM for the natural atomic linewidth.

(b) The rms atomic time-of-flight in the laser-beam overlap volume. For an rms velocity of 3×10^4 cm/sec and an estimated excitation radius of 5×10^{-3} cm, the associated linewidth is about 6 MHz.

(c) Optical field Stark broadening of the levels. For our peak laser intensity of about 1 kW/cm^2 the broadening may be estimated as roughly 2 kHz.

(d) Broadening of the atomic line as a result of collisions between the excited-state $7\,^2P_{1/2}$ atoms and ground-state $6^2P_{1/2}$ atoms.

Both (a) and (b) may contribute to the low-density linewidth; (c) is negligible. (b) is very weakly temperature dependent, while (d) is linear in

atomic density. We expect the self-broadening rate to be comparable to that of foreign-gas broadening, since the responsible collisions occur between atoms in states which are not coupled by an electric dipole moment.

The frequency scale of the linewidth measurements was calibrated in terms of our measured value of the $F=1\rightarrow1$ ^{203}Tl-^{205}Tl isotope shift. At each value of cell temperature, many single-sweep oscilloscope traces [similar to that of Fig. 9(c)] were taken. Those traces for which the line shape was asymmetric (evidently because of a rapid change of laser frequency during that particular sweep through the absorption line) were rejected. The linewidths of the others were measured and averaged. In Fig. 10 we have plotted the mean width w (FWHM) of the absorption line as a function of ground-state atomic thallium density N; the vapor-pressure curve of Honig[26] and the ideal-gas law were used to convert from cell temperature to atomic density. If we assume a linear dependence of linewidth w on density N, that is $w=w_0+\beta N$, we obtain the following from a least-squares fit of the mean measured values of w for each N: $w_0=6.50\pm0.35$ MHz, $\beta=(0.95\pm0.09)\times10^{-15}$ MHz cm^3. These uncertainties do not include the uncertainty in the value of thallium density associated with temperature nonuniformity in the cell and uncertainty in the vapor-pressure curve. The experimental values of $2w_0$ is in reasonable agreement with the estimate of residual broadening due to (a) and (b) above. At a temperature of 860°C, corresponding to a thallium vapor pressure of 1 Torr, the experimental value of 2β corresponds to an atomic self-broadening of 16 MHz/Torr, which is of the order of magnitude of typical foreign-gas-broadening coefficients,[27] as we expected. The corresponding collisional cross section is $2\pi\beta/\bar{v}=1.6\times10^{-13}$ cm^2, where $\bar{v}$ is the rms atomic velocity.

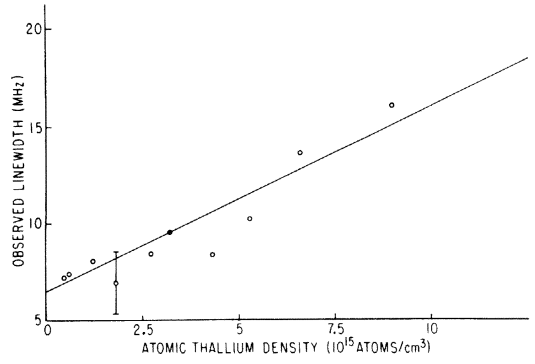

FIG. 10. Observed linewidth of the $6\,^2P_{1/2}$-$7\,^2P_{1/2}$ $F=1\rightarrow1$ ^{205}Tl TPA as a function of Tl vapor density. The inferred atomic linewidth is twice as large.

We did find that the linewidth could in fact be increased irreversibly by heating the cell to the temperature at which it was originally baked out. The atomic linewidth observed in a second thallium cell, the temperature of which had been raised above 1000°C several times, was found to be 60 MHz at the lowest temperature at which TPA could be observed in this cell (about 700°C). The appearance of this additional broadening, which is probably due to impurity gases outgassed from the cell surfaces at the higher temperatures, demonstrates the necessity of using clean cells for this type of experiment. A small impurity contribution to the linewidth $2w_0$ in our cleaner cell cannot be ruled out, either.

VIII. SUMMARY AND CLOSING REMARKS

We have measured isotope shifts, hyperfine splittings, magnetic field splitting, and nonresonant collisional self-broadening of the $7\,^2P_{3/2,\,1/2}$ states of thallium. We have also shown that it is quite feasible to make measurements by Doppler-free TPA using a cw single-mode laser even when the laser frequency is many thousands of cm^{-1} away from resonance with an intermediate state.

A good deal of improvement of the measurements is possible. If one uses a stable confocal Fabry-Perot interfermometer about 1 m long to analyze the laser spectrum during a laser-frequency sweep, one should be able to reduce the frequency-measurement uncertainties below 2 MHz.[13] Further improvement is possible using a double-resonance technique, with the laser simply used as a source of excitation on (two-photon) resonance, while suitably chosen dc and rf magnetic fields are applied to the atoms. In addition, the self-broadening measurements could be improved considerably and extended to collisional frequency shifts by simultaneously observing the TPA spectra of two cells containing different densities of thallium but irradiated by the same laser beam. Foreign-gas broadening and shifts could be measured by this method, as well.[42]

We emphasize that our analysis of the hfs constants of the $n\,^2P$ series of Tl indicates that the surprising result $A_{3/2}(n=7)>A_{3/2}(n=6)$ is not due to an anomaly in the $7\,^2P_{3/2}$ state. We find, in fact, that the hfs of the $7\,^2P$ states conforms rather well with previous measurements of the 8 and $9\,^2P$ states.[27(a)] It is the value of $A_{3/2}(n=6)$ which is anomalously small, apparently because the value of a_c for this state is positive and of the same order of magnitude as $a_{3/2}$. For the states $n=7, 8, 9$, however, this type of cancellation does not occur, apparently because a_c is negative for

these states. A theoretical calculation of a_c for the various terms of the ^2P series of thallium as a confirmation of our analysis would certainly be most desirable.

ACKNOWLEDGMENTS

In closing, we would like to thank Professor R. Gupta and Professor W. Happer for stimulating discussions. We are also indebted to Professor W. R. S. Garton of the Imperial College of London and Professor S. Svanberg of Chalmers University of Technology for bringing some previous work on thallium to our attention.

APPENDIX A: RELATIVE TPA RATES

Our goal in this appendix is to calculate the relative TPA rates for transitions between different Zeeman levels and for transitions between different hyperfine levels.

Let $\hat{\delta}$ and $\hat{\epsilon}$ be the unit polarization vectors of the incident beams of angular frequency ω_1 and ω_2, respectively. By assumption, the sum $\omega_1 + \omega_2$ is exactly equal to the transition frequency between the initial atomic state $|a\rangle$ and final state $|b\rangle$. The TPA rate is proportional to the absolute square of a polarizability $\mathcal{A}$ which, in the dipole approximation, is given by[28]

$$\mathcal{A} = \sum_{i,j} \delta_i \mathcal{A}_{ij} \epsilon_j ,$$

where

$$\mathcal{A}_{ij} = \frac{1}{\hbar} \sum_n \frac{\langle b|p_i|n\rangle\langle n|p_j|a\rangle}{\omega_{na} - \omega_2} + \frac{\langle b|p_j|n\rangle\langle n|p_i|a\rangle}{\omega_{na} - \omega_1} .$$

In the special case $\omega_1 = \omega_2 = \omega$, to which we will restrict ourselves here, we obtain

$$\mathcal{A}_{ij} = \frac{1}{\hbar} \sum_n \frac{\langle b|p_i|n\rangle\langle n|p_j|a\rangle + \langle b|p_j|n\rangle\langle n|p_i|a\rangle}{\omega_{na} - \omega} .$$

Here i and j are Cartesian coordinates, $\langle m|p_i|n\rangle$ is the ith component of the dipole matrix element between atomic states m and n of energies $\hbar\omega_m$ and $\hbar\omega_n$, respectively; $\omega_{na} \equiv \omega_n - \omega_a$, and $|a\rangle$, $|b\rangle$, and $|n\rangle$ are the initial, final, and intermediate atomic states, respectively. If the initial and final states contain degenerate levels, we must also sum $|\mathcal{A}|^2$ over them.

Following Placzek,[29] who treated the similar case of Raman scattering, we break $\mathcal{A}_{ij}$ up into a trace $\mathcal{A}^{(0)}$ and symmetric traceless part $\mathcal{A}^{(2)}_{ij}$ as follows:

$$\mathcal{A}_{ij} = \delta_{ij} \mathcal{A}^{(0)} + \mathcal{A}^{(2)}_{ij} ,$$

where

$$\mathcal{A}^{(0)} = \frac{1}{3} \sum_{i=1}^{3} \mathcal{A}_{ii} .$$

$\mathcal{A}^{(0)}$ and $\mathcal{A}^{(2)}$ are, respectively, the scalar and second-rank tensor components of $\mathcal{A}_{ij}$; the vector or first-rank component $\mathcal{A}^{(1)}$ is given by the antisymmetric part of $\mathcal{A}_{ij}$ and hence vanishes identically.[30]

Let the states $|a\rangle$ and $|b\rangle$ be characterized by the quantum numbers $\alpha J_a I F_a M_a$ and $\beta J_b I F_b M_b$, where I, J, and F denote the total angular momentum of the nucleus, electron, and atom, respectively, M denotes the component of F along a dc magnetic field $H_0 \hat{z}$, and α and β denote the other atomic quantum numbers. In addition, we define an operator A_{ij} whose matrix elements are the polarizability tensor $\mathcal{A}_{ij}$. Following the notation of Messiah,[31] we introduce the spherical components of the tensor, which we denote by Greek rather than Latin subscripts. We thus have

$$\mathcal{A} = \sum_{i,j=1}^{3} \delta_i \mathcal{A}_{ij} \epsilon_j = \sum_{\mu,\nu=0,\pm1} \delta_{-\mu} \epsilon_{-\nu} \mathcal{A}_{\mu\nu} (-1)^{\mu+\nu}$$

but

$$\mathcal{A}_{\mu\nu} = \sum_{J,M} \langle 11\mu\nu|JM\rangle \langle \beta J_b I F_b M_b | A^{(J)}_M | \alpha J_a I F_a M_a \rangle ,$$

where $\langle 11\mu\nu|JM\rangle$ is a Clebsch-Gordan coefficient, and $A^{(J)}_M$ is the Mth component of a spherical-tensor operator of rank J. Since the $A^{(J)}_{ij}$'s are linear combinations of the $A^{(J)}_M$'s, it is clear that the components of $A^{(1)}$ vanish identically.

Using the Wigner-Eckart theorem, we obtain

$$\mathcal{A} = \sum_{JM} (-1)^M \gamma^{(J)}_{-M} \langle \beta J_b I F_b \| A^{(J)} \| \alpha J_a I F_a \rangle \times (-1)^{2J} \langle F_a J M_a M | F_b M_b \rangle (2F_b + 1)^{-1/2}, \quad \text{(A1)}$$

where

$$(-1)^M \gamma^{(J)}_{-M} = \sum_{\mu,\nu} \langle 11\mu\nu|JM\rangle \delta_{-\mu} \epsilon_{-\nu} (-1)^{\mu+\nu} . \quad \text{(A2)}$$

Since the tensor operator $A^{(J)}$ is independent of nuclear spin,[32] it follows from Eq. (A1) that

$$\mathcal{A} = \sum_{JM} (-1)^M \gamma^{(J)}_{-M} \langle \beta J_b \| A^{(J)} \| \alpha J_a \rangle \times (-1)^{F_a + J_a + J_b - J} (2F_a + 1)^{1/2} \times \langle F_a J M_a M | F_b M_b \rangle \begin{Bmatrix} J_a & J & J_b \\ F_b & I & F_a \end{Bmatrix} , \quad \text{(A3)}$$

where the symbol in curly brackets is a 6-J symbol, while the double-lined matrix elements denote reduced matrix elements. From the 6-J symbol the selection rules $|J_b - J_a| \le J \le J_b + J_a$ and $|F_b - F_a| \le J \le F_b + F_a$ may be deduced. Thus, for example, the $J = 0$ term vanishes unless $J_b = J_a$ and $F_b = F_a$, while the $J = 2$ term vanishes if $J_a + J_b < 2$. Some of these TPA selection rules have been noted previously.[33]

Applying these rules to TPA in thallium ($I=\frac{1}{2}$), we find that only the scalar polarizability ($J=0$) contributes to the $6\,^2P_{1/2}$-$7\,^2P_{1/2}$ TPA. Thus only the transitions $F=0\rightarrow 0$ and $1\rightarrow 1$ are allowed, and since only $M=0$ appears in the sum in Eq. (A3), it follows that only transitions in which $M_a=M_b$ may occur. On the other hand, only the traceless polarizability ($J=2$) contributes to the $6\,^2P_{1/2}$-$7\,^2P_{3/2}$ TPA. The possible transitions are now $F=0\rightarrow 2$, $1\rightarrow 1$, and $1\rightarrow 2$. In general, there are no restrictions on M_a and M_b, except for those implicit in the polarization coefficients $\gamma^{(J)}_{-M}$.

Equation (A3) may be used to calculate relative TPA rates in the presence of a weak dc magnetic field $H_0\hat{z}$. We will restrict our analysis to the $6\,^2P_{1/2}$-$7\,^2P_{1/2,\,3/2}$ thallium transitions which we have observed experimentally.

We consider the possible splitting of the $F=1\rightarrow 1$ $6\,^2P_{1/2}$-$7\,^2P_{1/2}$ ($M=-1\rightarrow -1, 0\rightarrow 0, 1\rightarrow 1$) transition in a weak field. We note immediately that only the principal quantum number n changes in the TPA. Since to a very good approximation (LS coupling) the splitting in a weak magnetic field is independent of n,[34] we conclude that the $F=1\rightarrow 1$ transition is not split, even though the state degeneracy is lifted by the field. This situation is similar to that observed in Na ($3S$-$5S$ TPA) by Bloembergen.[16]

On the other hand, the $6\,^2P_{1/2}$-$7\,^2P_{3/2}$ transition will be split in a weak field, since $J_a\neq J_b$. If we neglect the nuclear magnetic moment and assume LS coupling, the weak-field perturbation energy ΔW (measured in Hz) of a level having quantum numbers $LSJFM$ is $\mu_B H_0 g M/h$, where

$$g=g_J[F(F+1)+J(J+1)-I(I+1)][2F(F+1)]^{-1}. \tag{A4}$$

Here g_J is the Landé g factor,[34] μ_B is the Bohr magneton (1.38 MHz/G), and L and S represent the quantum numbers of orbital and spin angular momentum of the atomic state. From Eq. (A4) we obtain g factors of 1, $\frac{5}{3}$, and $\frac{1}{3}$ in the $7\,^2P_{3/2}$ $F=2$, $7\,^2P_{3/2}$ $F=1$, and $6\,^2P_{1/2}$ $F=1$ states, respectively.

We may now calculate the relative TPA rates of various Zeeman-level $6\,^2P_{1/2}$-$7\,^2P_{3/2}$ transitions, which, according to Eq. (A3), are proportional to $|\gamma^{(J)}_{-M}|^2\,\langle F_a\,2M_aM|F_bM_b\rangle^2$. For simplicity we consider the case $\hat{\delta}=\hat{\epsilon}=\hat{x}$, that is, linearly polarized light in a plane perpendicular to the magnetic field. A straightforward calculation yields

$$|\gamma^{(2)}_{\pm M}|^2=(\tfrac{1}{6},\,0,\,\tfrac{1}{4})\quad(0\leq|M|\leq 2)\,. \tag{A5}$$

The relative TPA rates for linearly polarized light are given in Table IV. For arbitrary elliptical laser polarizations normal to the magnetic field Eq. (A5) should be replaced by

$$|\gamma^{(2)}_0|^2=\tfrac{1}{6}|\hat{\delta}\cdot\hat{\epsilon}|^2,\quad |\gamma^{(2)}_{\pm 1}|^2=0,\quad |\gamma^{(2)}_{\pm 2}|^2=|\delta_{\mp}\epsilon_{\mp}|^2. \tag{A6}$$

Note that $M=\pm 1$ transitions are forbidden, since each of the two photons must contribute either $+1$ or -1 units of angular momentum to the atom undergoing the transition.

We now consider the general calculation of relative TPA rates of different hyperfine multiplets for arbitrary polarizations $\hat{\delta}$ and $\hat{\epsilon}$. Squaring Eq. (A3), summing over M_a and M_b and making use of a Clebsch-Gordan orthogonality relationship, we obtain

$$\sum_{M_aM_b}|\mathcal{A}|^2=\sum_{JM}(-1)^M\gamma^{(J)}_{-M}\gamma^{(J)}_{M}|\langle\beta J_b||A^{(J)}||\alpha J_a\rangle|^2 \times(2F_a+1)(2F_b+1)(2J+1)^{-1}\begin{Bmatrix} J_a & J & J_b\\ F_b & I & F_a\end{Bmatrix}^2. \tag{A7}$$

For transitions for which either the $J=0$ or $J=2$ terms (but not both) contribute (because of the selection rules implicit in the 6-J symbol), the relative TPA rates are simply proportional to the square of the appropriate 6-J symbol multiplied by $(2F_a+1)(2F_b+1)$.[35] For $J=0$ this factor reduces to $(2F_a+1)(2J_a+1)^{-1}\delta_{J_aJ_b}\delta_{F_aF_b}$; for $J=2$ it is most convenient to look up the 6-J symbol in a table.[36]

Applying these results to Tl, we find that for the $6\,^2P_{1/2}$-$7\,^2P_{1/2}$ TPA, the $F=0\rightarrow 0$ and $1\rightarrow 1$ absorption rates are in the ratio 1:3, while in the $6\,^2P_{1/2}$-$7\,^2P_{3/2}$ TPA, the $F=0\rightarrow 2$, $1\rightarrow 1$, and $1\rightarrow 2$ absorption rates are in the ratio 2:3:3. The same

TABLE IV. $6\,^2P_{1/2}$-$7\,^2P_{3/2}$ Zeeman splitting and relative TPA rates for linearly polarized excitation.

Multiplet	$M_a\rightarrow M_b$	Relative TPA rate	Relative position[a]
$F=0\rightarrow 2$	$0\rightarrow 0$	4	0
	$0\rightarrow\pm 2$	6	± 6
$F=1\rightarrow 1$	$0\rightarrow 0$	4	0
	$\pm 1\rightarrow\mp 1$	9	∓ 6
	$\pm 1\rightarrow\pm 1$	1	± 4
$F=1\rightarrow 2$	$0\rightarrow 0$	0[b]	0
	$0\rightarrow\pm 2$	6	± 6
	$\pm 1\rightarrow\mp 1$	3	∓ 4
	$\pm 1\rightarrow\pm 1$	3	± 2

[a] Units are $\frac{1}{3}\mu_B H_0$, where $\mu_B=1.38$ MHz/G, and H_0 is the applied axial magnetic field.

[b] Vanishing of this matrix element is not due to any simple selection rule.

conclusions follow from intensity sum rules[34] applied to transitions between the hyperfine multiplets.

In the most general case of TPA, both the $J=0$ and $J=2$ terms contribute, and therefore it may be expedient to have an explicit expression for the reduced matrix elements in terms of reduced dipole matrix elements:

$$|\langle \beta J_b \| A^{(J)} \| \alpha J_a \rangle|^2 = 4(2J+1) \left| \sum_n \begin{Bmatrix} J_b & J_a & J \\ 1 & 1 & J_n \end{Bmatrix} \frac{\langle \beta J_b \| p \| n J_n \rangle \langle n J_n \| p \| \alpha J_a \rangle}{\hbar(\omega_{na} - \omega)} \right|^2 . \tag{A8}$$

The polarization coefficients may also be calculated explicitly as

$$|\gamma_0^{(0)}|^2 = \tfrac{1}{3} |\hat{\delta} \cdot \hat{\epsilon}|^2 ,$$

$$\sum_M \gamma_M^{(2)} \gamma_{-M}^{(2)} (-1)^M = \tfrac{1}{2} + \tfrac{1}{2} |\hat{\delta}^* \cdot \hat{\epsilon}|^2 - \tfrac{1}{3} |\hat{\delta} \cdot \hat{\epsilon}|^2 .$$

Finally, we note that the magnitude of a dipole matrix element $\langle \beta J_b \| p \| n J_n \rangle$ may often be evaluated from experimentally measured values of the line strength $S(\beta J_b \to n J_n)$ or oscillator strength $f(nJ_n, \beta J_b)$:[37]

$$|\langle \beta' J_b \| p \| n J_n \rangle|^2 = S(\beta J_b \to n J_n) = \tfrac{3}{4} r_e \hbar c^2 (2J_b + 1) \omega_{nb}^{-1} f(nJ_n, \beta J_b),$$

where r_e is the classical electron radius. However, the sign of the product of reduced dipole matrix elements $\langle \beta J_b \| p \| n J_n \rangle \langle n J_n \| p \| \alpha J_\alpha \rangle$ is quite often unmeasured,[38,39] even when the magnitude is known.

APPENDIX B: ESTIMATION OF THE TPA RATE

Noting that in our experiment the incident laser frequency is some 8000 cm^{-1} away from the nearest single-photon resonance, as opposed to only 400 cm^{-1} in sodium, we see that the thallium cross section for TPA should be lower by a factor of about $(\frac{8000}{400})^2 \cong 400$ than that of Na. Clearly, however, this reduction may be compensated for by using an atomic thallium density several orders of magnitude larger than that used in the sodium TPA experiment.

We can estimate the Doppler-free TPA rate as follows: For an incident laser beam of angular frequency ω and intensity I (ergs/cm^2 sec), the Doppler-free TPA rate by a single atom having resonance frequency $\omega_0 \cong 2\omega$ may be written[40]

$$\Gamma(\omega) = [4\pi^3/(\hbar c)^2] g(2\omega - \omega_0) |\mathfrak{A}|^2 I^2 , \tag{B1}$$

where $\mathfrak{A}$ is a polarizability defined in Appendix A, and $g(2\omega - \omega_0)$ is a line-shape factor normalized to 1; e.g., if the transition linewidth is Lorentzian and is determined by the lifetime of the excited state then $g(0) = 2/\pi\gamma$, where γ is the inverse lifetime of the excited state. For perfect overlap between two opposing Gaussian laser beams, each having power P and a (coincident) minimum waist r_0, integration of Eq. (B1) over all space yields the following value for the number of atoms, dn/dt excited per second within a vapor containing N atoms/cm^3 in a single nondegenerate state:

$$\frac{dn}{dt} = 2\pi^3 N |\mathfrak{A}|^2 P^2 \omega g(2\omega - \omega_0)/\hbar^2 c^3 . \tag{B2}$$

This result, which is independent of r_0, holds in the limit in which the longitudinal extent $l \equiv 2r_0^2\omega/c$ of the laser beam is much smaller than the length of the vapor, so that the most intense part of the beam is contained within the vapor.[41]

For the $6\,^2P_{1/2} \to 7\,^2P_{1/2,\,3/2}$ TPA in thallium we have $\omega/2\pi c = 3.5 \times 10^4$ cm^{-1}, and we estimate $\mathfrak{A}$ to be roughly 3×10^{-25} cm^3. Thus, for $g(0) \cong 10^{-8}$ sec (including laser frequency jitter), a power of $P = 10^6$ ergs/sec^{-1} (0.1 W) should yield an excitation rate dn/dt of 4×10^9 sec^{-1} at a number density $N = 2 \times 10^{14}$ cm^{-3} (about 0.1 Torr of thallium). Taking into account the solid angle within which the fluorescence was observed, the transmission of the collection optics, and the detector quantum efficiency, we expect a signal of about 4×10^5 photoelectrons/sec on two-photon resonance. The magnitude of the experimental signal was comparable with this estimate.

*Work supported by the Joint Services Electronics Program (U.S. Army, U.S. Navy, and U.S. Air Force) under Contract DAAB07-74-C-0341, and by the National Science Foundation under Grant NSF-DMR 73-07600 A02.

[1]H. B. G. Casimir, *On the Interaction between Atomic Nuclei and Electrons* (Freeman, New York, 1963).
[2]H. Kopfermann, *Nuclear Moments* (Academic, New York, 1958).
[3]E. Fermi and E. Segrè, Reale Accademia d'Italia IV, 131 (1933); Z. Phys. 82, 729 (1933).
[4]Charles Schwartz, Phys. Rev. 105, 173 (1957).
[5]Gordon Gould, Phys. Rev. 101, 1828 (1956).
[6]A. I. Odintsov, Opt. Spectrosc. (USSR) 9, 75 (1960).
[7]L. S. Vasilenko, V. P. Chebotaev, and A. V. Shishaev, JETP Lett. 12, 113 (1970).
[8]A. Flusberg, T. Mossberg, and S. R. Hartmann, Phys. Lett. 55A, 403 (1976).
[8(a)]W. R. S. Garton, E. M. Reeves, and F. S. Tomkins, Proc. R. Soc. Lond. A 341, 163 (1974); P. Zimmermann, Z. Phys. 232, 32 (1970).

[8(b)]M. Brieger, H. Bucka, A. Reichelt, and P. Zimmermann, Z. Naturforsch, 24a, 903 (1969).
[9]C. J. Schuler, M. Çiftan, L. C. Bradley, III, and H. H. Stroke, J. Opt. Soc. Am. 52, 501 (1962).
[10]Wolfgang Fischer, Fortschr. Phys. 18, 89 (1970).
[11]F. Biraben, B. Cagnac, and G. Grynberg, Phys. Rev. Lett. 32, 643 (1974).
[12]M. D. Levenson and N. Bloembergen, Phys. Rev. Lett. 32, 645 (1974).
[13]T. W. Hänsch, K. C. Harvey, G. Meisel, and A. L. Schawlow, Opt. Commun. 11, 50 (1974).
[14]K. C. Harvey, R. T. Hawkins, G. Meisel, and A. L. Schawlow, Phys. Rev. Lett. 34, 1073 (1975).
[15]P. F. Liao and J. E. Bjorkholm, Phys. Rev. Lett. 34, 1 (1975).
[16]N. Bloembergen, M. D. Levenson, and M. M. Salour, Phys. Rev. Lett. 32, 867 (1974).
[17]A. Lurio and A. G. Prodell, Phys. Rev. 101, 79 (1956).
[18]A. Landé, Z. Phys. 25, 46 (1924).
[19]W. G. Proctor, Phys. Rev. 79, 35 (1950).
[20]D. R. Hartree, Proc. Camb. Philos. Soc. 24, 426 (1928).
[21]Charlotte Moore, *Atomic Energy Levels*, Natl. Bur. Stand. (U.S.) Circular 467 (U.S. GPO, Washington, D.C., 1958).
[22]R. Sternheimer, Phys. Rev. 86, 316 (1952).
[23]The uncertainty of the sign of the spin polarization has also been discussed by Melba Phillips [Phys. Rev. 103, 322 (1956)].
[24]Ingvar Lindgren and Arne Rosén, Case Studies At. Phys. 4, 197 (1974).
[25]D. R. Bates and Agnete Damgaard, Philos. Trans. R. Soc. Lond. A 242, 101 (1949).
[26]R. E. Honig and D. A. Kramer, RCA Rev. 30, 285 (1969).
[27]Shang-Yi Ch'en and Makoto Takeo, Rev. Mod. Phys. 29, 20 (1957).
[27(a)]The ratio of the isoelectronic Bi III 7^2P states hyperfine constants [S. Goudsmit, Phys. Rev. 37, 1057 (1931)] is also found to agree well with the prediction of the semiempirical theory (see Ref. 10). However, the Bi III $6^2P_{3/2}$ state hyperfine constant has not, as far as we know, been measured. Thus it is not known whether the magnitude of the $n^2P_{3/2}$ hyperfine constant of Bi III increases when n is increased from 6 to 7.
[28]Maria Göppert-Mayer, Ann. Phys. (Leipz.) 9, 273 (1931).
[29]G. Placzek, Handbuch der Radiologie VI, 2, Akademische Verlagsgesellschaft, Leipzig, 1934 (English translation: UCRL Translation 526L, U.S. AEC) (unpublished).
[30]Note that for the case $\omega_1 \neq \omega_2$ $\mathfrak{A}^{(1)}$ is nonzero, since $\mathfrak{A}_{ij}$ is not symmetric in i and j. Even for $\omega_1 = \omega_2$ there is a small component of $\mathfrak{A}^{(1)}$ associated with the fact that these frequencies are not quite equal in the rest frame of an atom of arbitrary velocity.
[31]Albert Messiah, *Quantum Mechanics* (Wiley, New York, 1966), Vol. II.
[32]This independence holds only in the limit in which $\omega - \omega_{na}$ is much greater than the hyperfine splitting of the intermediate state $|n\rangle$ (for all n).
[33]B. Cagnac, G. Grynberg, and F. Biraben, J. Phys. (Paris) 34, 845 (1973).
[34]E. U. Condon and G. H. Shortley, *The Theory of Atomic Spectra* (Cambridge U.P., Cambridge, 1967).
[35]F. Biraben, E. Giacobino, and G. Grynberg, Phys. Rev. A 12, 2444 (1975).
[36]See, for example, M. Rotenberg, R. Bivins, N. Metropolis, and J. K. Wooten, Jr., *The 3-J and 6-J Symbols* (Technology, MIT, Cambridge, Mass., 1959).
[37]E. U. Condon and G. H. Shortley, Ref. 34. Note, however, that our reduced dipole matrix element is that of Messiah, Ref. 31.
[38]L. Vriens, Opt. Commun. 11, 396 (1974).
[39]A. Flusberg, thesis (Columbia University, 1975) (unpublished).
[40]See, for example, Ref. 33.
[41]See Ref. 13.
[42]*Note added in proof.* It has come to our attention that a foreign-gas broadening and pressure shift TPA experiment of the type suggested in Sec. VIII has been reported in Na vapor [F. Biraben, B. Cagnac, and G. Grynberg, J. Phys. (Paris) 36, L41 (1975)].

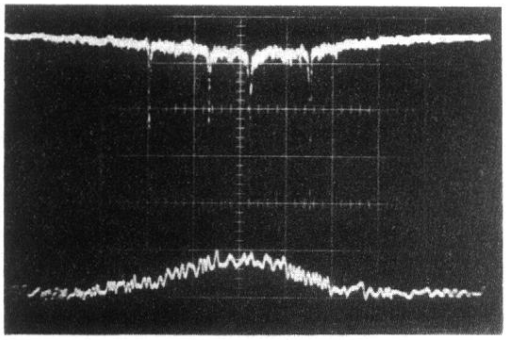

FIG. 3. *Upper trace*: 535-nm fluorescence as a function of dye-laser frequency (increasing to the right), showing the $6\,^2P_{1/2}$-$7\,^2P_{3/2}$ TPA spectrum ($F = 1 \rightarrow 1$ and $1 \rightarrow 2$ only). Horizontal scale: 240 MHz/div. The smaller (larger) peaks correspond to ^{203}Tl (^{205}Tl). (Cf. Fig. 5). Note the Doppler-broadened backround. *Lower trace*: Transmission of the dye laser through an iodine vapor cell; again note the Doppler-broadened absorption. Both traces were obtained on a single sweep (at about 20 msec/div) of the dye-laser frequency, as observed on a dual-beam oscilloscope.

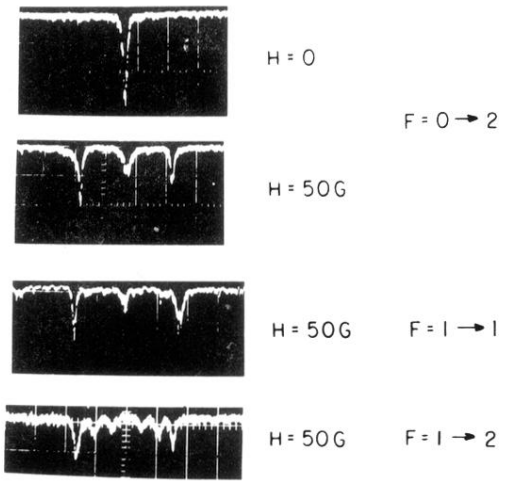

FIG. 9. ^{205}Tl $6\,^2P_{1/2}$-$7\,^2P_{3/2}$ TPA splitting in a weak axial magnetic field H for the three possible multiplet transitions. Each oscilloscope trace represents a single sweep of the laser frequency, increasing to the right at approximately 38 MHz/div. Time scale: 2 msec/div.